*Case Report*

# *Strongyloides stercoralis* Infestation in a Child: How a Nematode Can Affect Gut Microbiota

Stefania Pane [1], Anna Sacco [1], Andrea Iorio [2], Lorenza Romani [3] and Lorenza Putignani [2,*]

1   Department of Diagnostic and Laboratory Medicine, Unit of Parasitology, Bambino Gesù Children's Hospital, IRCCS, 00165 Rome, Italy; stefania.pane@opbg.net (S.P.); anna.sacco@opbg.net (A.S.)
2   Department of Diagnostic and Laboratory Medicine, Unit of Parasitology and Multimodal Laboratory Medicine Research Area, Unit of Human Microbiome, Bambino Gesù Children's Hospital, IRCCS, 00165 Rome, Italy; andrea.iorio@opbg.net
3   Immunology and Infectious Diseases Unit, University Department of Pediatrics, Bambino Gesù Children's Hospital, IRCCS, 00165 Rome, Italy; lorenza.romani@opbg.net
*   Correspondence: lorenza.putignani@opbg.net; Tel.: +39-06-6859-4127

**Abstract:** *Background:* Strongyloidiasis is a neglected tropical disease caused by the intestinal nematode *Strongyloides stercoralis* and characterized by gastrointestinal and pulmonary involvement. We report a pediatric case of strongyloidiasis to underline the response of the host microbiota to the perturbation induced by the nematode. *Methods:* We performed a 16S rRNA-metagenomic analysis of the gut microbiota of a 7-year-old female during and after *S. stercolaris* infection, investigating three time-point of stool samples' ecology: $T_0$- during parasite infection, $T_1$- a month after parasite infection, and $T_2$- two months after parasite infection. Targeted-metagenomics were used to investigate ecology and to predict the functional pathways of the gut microbiota. *Results:* an increase in the alpha-diversity indices in $T_0$-$T_1$ samples was observed compared to $T_2$ and healthy controls (CTRLs). Beta-diversity analysis showed a shift in the relative abundance of specific gut bacterial species from $T_0$ to $T_2$ samples. Moreover, the functional prediction of the targeted-metagenomics profiles suggested an enrichment of microbial glycan and carbohydrate metabolisms in the $T_0$ sample compared with CTRLs. *Conclusions:* The herein report reinforces the literature suggestion of a putative direct or immune-mediated ability of *S. stercolaris* to promote the increase in bacterial diversity.

**Keywords:** Strongyloidiasis; *Strongyloides stercoralis*; gut microbiota; targeted-metagenomics; host-parasite-microbiota interaction

## 1. Introduction

Strongyloidiasis is considered a neglected tropical disease caused by the intestinal nematode *Strongyloides stercoralis* and characterized by gastrointestinal (GI) and/or pulmonary involvement, with an estimated global prevalence of about 350 million cases [1]. It is endemic in the tropical and subtropical regions of the world where human wastes contaminate the environment, but it is widespread in Europe and in hypo-endemic areas in Italy [2,3]. Once the larvae penetrate the skin, they reach the bloodstream and invade the lungs' alveoli and this pulmonary migration may cause pneumonia, but usually in an asymptomatic way. The larvae are then expectorated, traveling through the trachea and then swallowed. The larvae mature and become adult parthenogenetic females, which release eggs into the GI tract. The eggs hatch while still in the GI tract and give rise to rhabditoid larvae, which are excreted. However, some of these larvae become infectious (filarioid) and penetrate the anal mucosa and perianal skin, re-entering the circulatory system and restarting the cycle. Because of this auto-infection cycle, a person can be infected with *S. stercoralis* for decades [4].

In immunocompetent subjects, the infection is usually asymptomatic, with low minimal and intermittent larval excretion and may bring a combination of uncertain clinical

symptoms such as severe epigastric pain, chronic diarrhea, constipation, indigestion, anorexia, anal pruritus, abdominal distension, weight loss, nausea, vomiting, peripheral eosinophilia, asthenia, adynamia, fever, hemorrhage, anemia, and, rarely, obstruction of the small intestine [5,6].

However, in some predisposing conditions, such as initiation of immunosuppressive therapy and kidney transplant recipients, the disease may change to any form of hyper-infection or disseminated types of strongyloidosis [7].

Herein, we report a pediatric case of *S. stercoralis* hyper-infection, for which larval forms were characterized in stool samples of an asymptomatic patient with a nephrotic syndrome. The parasitological diagnosis was based on light microscopy, molecular PCR-based investigation, and serology. Coupled with parasitological exams, a stool time-point sampling underwent to assess microbiota modulation in terms of ecology and global composition, comparing the patient's gut microbiota during the infection, post-infection, and using reference, age-matched healthy subjects as controls (CTRLs). This study was conducted to describe the response of the host microbiota to the perturbations induced by the nematode pathogen.

## 2. Results

### 2.1. Morphology-Based and PCR-Based Methods for the Identification of S. stercoralis

By examining stools under light microscopy, a large number of rhabditiform larvae of *S. stercoralis* were identified. The identification of larvae (L3) of *S. stercoralis* was based on nematode morphological features: (i) long esophagus, with a visible bowel junction, (ii) pointed tail, and (iii) mouthparts. Rhabditiform larvae were 250–280 mm in length, with a relatively short, but pointed tail, and a buccal cavity (Figure 1, panels A and B).
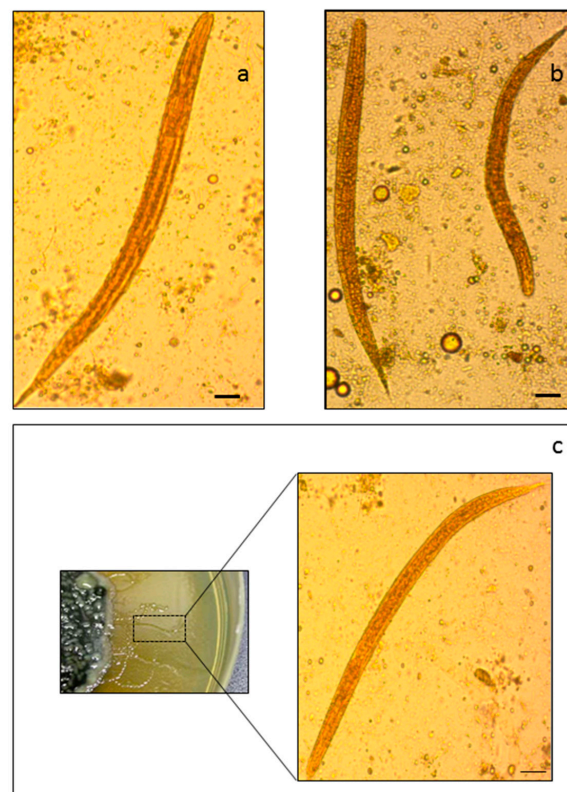


**Figure 1.** Light microscope-based characterization of *Strongyloides stercoralis*. Rhabditiform larvae of *S. stercoralis* are reported in panels (**a–c**) at 40× magnification. The inset refers to a larva onto an agar plate.

The agar plate culture technique was conducted on positive stool specimens and, after seven days, the sealed plates were examined under the 20× microscope objective and motile larvae actively moving were observed under a 40× objective (Figure 1, panel C).

Moreover, DNA amplification of *S. stercoralis* was successfully obtained in this positive stool sample using species-specific primers, thus, confirming the microscopic examination (data not shown).

According to the microscopic and molecular PCR-based investigation, patient serology also resulted in a positive. Instead, microscopic examination of the multiple bronchial washings and CSF samples appeared negative.

### 2.2. Gut Microbiota Profiling Associated with S. stercoralis Infection

2.2.1. Shaping of Patient's Gut Microbiota Ecology

We monitored the patient's gut microbiota shaping since the nematode infection to the second month of negative stool samples, relying on three time-points of stool sampling ($T_0$: during parasite infection, $T_1$: a month after parasite infection, and $T_2$: two months after parasite infection). A total of 1,718,328 high-quality reads were obtained from the $T_0$, $T_1$, and $T_2$ samples, and 16 stool samples from healthy, age-matched individuals, with a mean of 85,916 high-quality reads per sample, were used as a gut microbiota reference for comparisons.

The number of OTUs detected at each time-point sample ranged from 1365 to 790, highlighting a decrease of the gut microbiota diversity from parasite infection ($T_0$) to post-infection ($T_2$) time points (Table 1).

**Table 1.** Summary of the analyzed samples for the gut microbiota profiling and sequencing output.

| SAMPLE_ID | STATUS | Age | Total Reads Count (N) | Assigned Reads (N) | OTUs (N) |
|---|---|---|---|---|---|
| $T_0$ | During parasite infection | 7 | 53,476 | 36,643 | 1365 |
| $T_1$ | 1 month after parasite infection | 7 | 16,830 | 14,598 | 917 |
| $T_2$ | 2 months after parasite infection | 7 | 44,876 | 42,857 | 790 |
| N-05-1 | healthy control | 7–8 | 58,775 | 57,578 | 1062 |
| N-05-2 | healthy control | 7–8 | 68,144 | 61,598 | 1475 |
| N-05-3 | healthy control | 7–8 | 54,796 | 52,930 | 799 |
| N-05-4 | healthy control | 7–8 | 164,725 | 159,772 | 1044 |
| N-05-5 | healthy control | 7–8 | 84,616 | 80,331 | 645 |
| N-05-6 | healthy control | 7–8 | 293,539 | 285,209 | 978 |
| N-05-7 | healthy control | 7–8 | 29,696 | 29,454 | 377 |
| N-05-8 | healthy control | 7–8 | 40,400 | 37,790 | 875 |
| N-05-9 | healthy control | 7–8 | 76,140 | 75,780 | 463 |
| N-06-1 | healthy control | 7–8 | 60,591 | 60,217 | 397 |
| N-06-2 | healthy control | 7–8 | 46,304 | 46,014 | 455 |
| N-06-3 | healthy control | 7–8 | 400,539 | 393,198 | 1647 |
| N-06-4 | healthy control | 7–8 | 69,989 | 69,092 | 385 |
| N-06-5 | healthy control | 7–8 | 75,864 | 72,235 | 781 |
| N-06-6 | healthy control | 7–8 | 40,312 | 39,751 | 932 |
| N-06-7 | healthy control | 7–8 | 9379 | 9302 | 320 |
| N-06-8 | healthy control | 7–8 | 29,337 | 26,571 | 494 |

This decrease of the gut microbiota diversity from $T_0$ to $T_2$ was also confirmed by the calculation of the alpha-biodiversity indices. As shown in Figure 2, the $T_0$, $T_1$, and

$T_2$ alpha-diversity indices are included in the variability range of the healthy controls. However, $T_0$ and $T_1$ samples showed higher alpha-diversity values than the $T_2$ sample and the average of control groups.
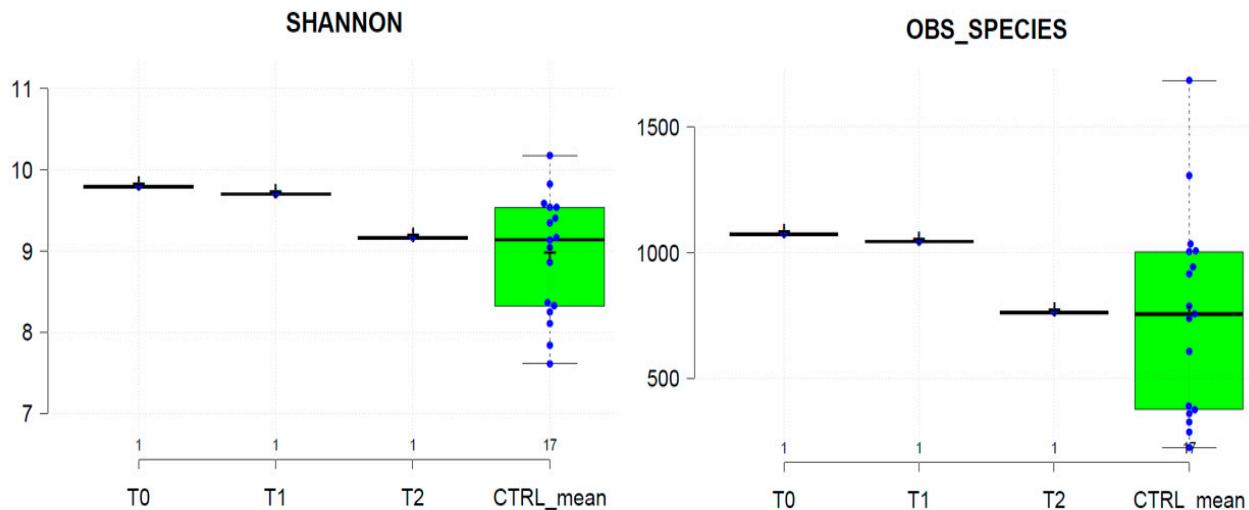


**Figure 2.** Alpha-diversity metrics of patient's gut microbiota at $T_0$, $T_1$, $T_2$, and healthy CTRL group (CTRL_mean). Left and right panels show Shannon and Observed_Species diversity indexes, respectively. Center lines show median values and box limits indicate the 25th and 75th percentiles.

A diverse range of bacterial phyla (L2) were identified in stool samples from the patient and healthy controls, including Bacteroidetes, Firmicutes, Proteobacteria, Verrucomicrobia, and Actinobacteria. In the gut microbiota from controls, Firmicutes were mostly prevalent (57.00%), followed by Bacteroidetes (15.90%), Actinobacteria (7.49%), Proteobacteria (3.86%), Verrucomicrobia (3.66%), and others (12.09%). Compared to CTRLs, the relative proportions of these phyla were mostly maintained in the $T_2$ sample. Instead, a clear shift in phyla proportions was observed in the $T_0$ and $T_1$ samples. Particularly, the $T_0$ and $T_1$ samples were depleted in Actinobacteria and enriched in Firmicutes with respect to the $T_2$ sample and CTRLs, as reported in the heatmap with hierarchical clustering of Figure 3.

At family (L5) and genus (L6) levels, the proportion of several bacterial families and genera were mostly similar between the $T_1$ and $T_2$ samples by clustering with the CTRLs, while the $T_0$ sample showed a different and specific gut microbiota pattern (Figures 4 and 5). In particular, at family level (L5), Bifidobacteriaceae, Coriobacteriaceae, Rikenellaceae, Clostridiaceae, Erysipelotrichaceae, and Ruminococcaceae, showed a gradual enrichment from the $T_0$ to the $T_2$ time-points. Meanwhile, Veillonellaceae, Staphylococcaceae, Lactobacillaceae, and Lachnospiraceae displayed a gradual depletion from the $T_0$ to the $T_2$ samples (Figure 4).

At genus level (L6), *Bifidobacterium*, *Blautia*, *Ruminococcus*, *Bacteroides*, *Corynebacterium*, *Colinsella*, *Streptococcus*, *Coprococcus*, and *Oscillospora* showed a gradual enrichment from the $T_0$ to $T_2$ time-points. Instead, *Staphylococcus*, *Lactobacillus*, and *Pediococcus* displayed a gradual depletion from the $T_0$ to $T_2$ samples (Figure 5).
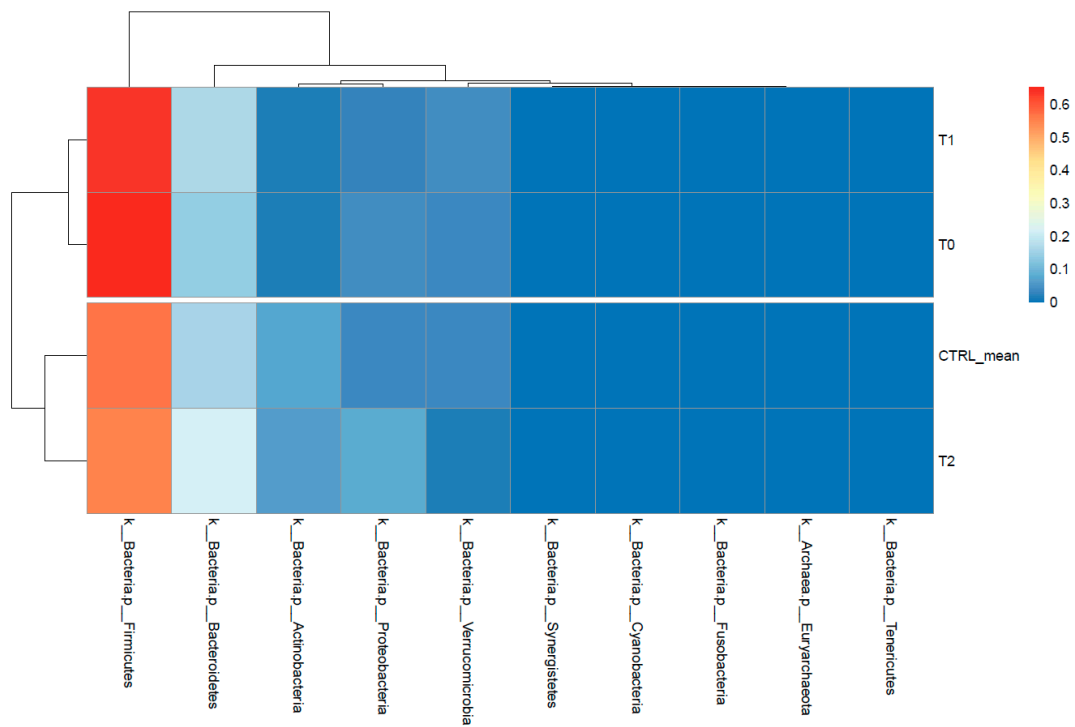
**Figure 3.** Heatmap with hierarchical clustering based on phyla (L2) abundances. The colors in the heatmap refer to the phylum's abundance, according to the color scale on the right.
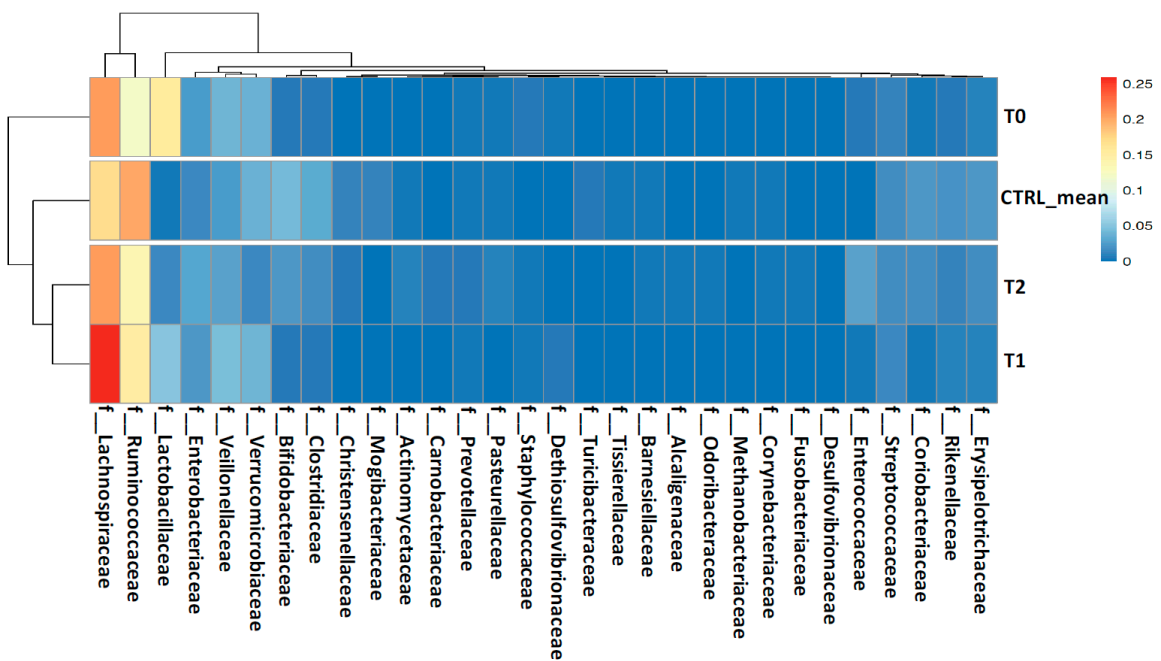


**Figure 4.** Heatmap with hierarchical clustering based on families' (L5) abundances. The colors in the heatmap refer to the family's abundance, according to the color scale on the right.
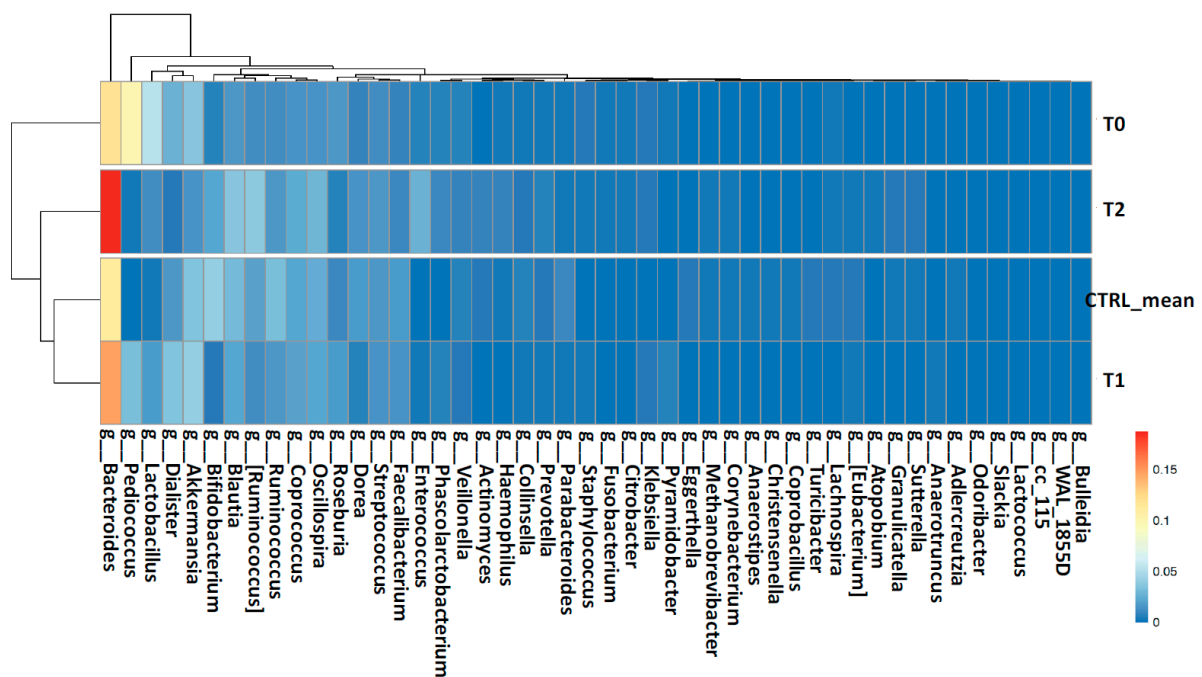
**Figure 5.** Heatmap with hierarchical clustering based on genera (L6) abundances. The colors in the heatmap refer to the genus abundance, according to the color scale on the right.

The gut microbiota biodiversity between the three patient's time-point samples and CTRLs was also analyzed via beta-diversity. According to the previous results highlighted by hierarchical clustering, this analysis revealed a shaping of the patient's gut microbiota during ($T_0$) and after ($T_1$ and $T_2$) nematode infection, with the $T_1$ sample close to the $T_0$ and the $T_2$ sample shifted to the controls (Figure 6).
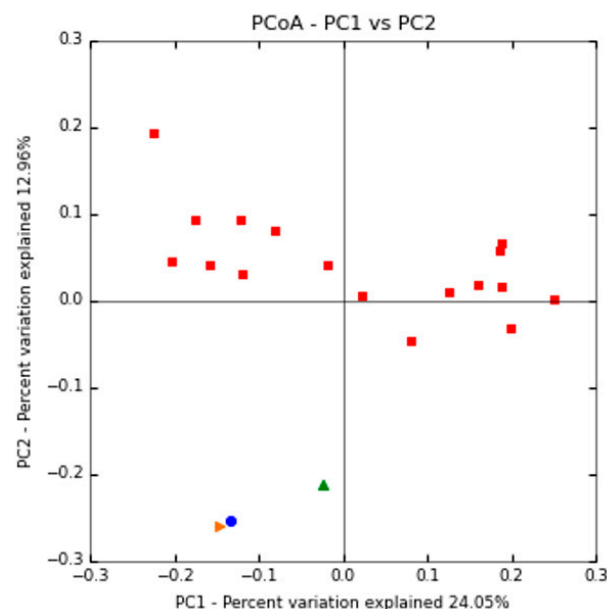


**Figure 6.** PCoA of beta-diversity values based on Bray Curtis distances. Patient gut microbiota at $T_0$: blue circle, $T_1$: orange triangle, $T_2$: green triangle, and healthy controls: red squares.

### 2.2.2. Metabolic Prediction of the Patient's Gut Microbiota during *S. stercoralis* Infection

To correlate the fecal microbiota composition data and inferred changes in bacterial metabolism with the response to the parasitic helminth infection, we conducted a predictive metagenomics analysis using PICRUSt. Functional prediction suggested that there were

differences in the bacterial functional content of the $T_0$ gut microbiota with respect to the healthy controls.

At KEGG level I (Figure 7), "Genetic Information Processing" pathway was depleted in the $T_0$ sample with respect to the controls and, for this reason, the prediction analysis of this pathway was further deepened by KEGG level II and III. At KEGG level II (Figure 8), "Cellular processes and Signaling," "Glycan Biosynthesis and Metabolism," "Carbohydrate Metabolism," "Signal Transduction," and "Cell Motility" pathways were enriched in the $T_0$ sample with respect to the controls. "Nucleotide Metabolism," "Amino Acid Metabolism," "Translation," "Transcription," and "Replication and Repair" were depleted in the $T_0$ sample when compared with the controls. At KEGG level III (Figure 9), "Transcription factors" and "Chaperons and folding catalysts" pathways were enriched in the $T_0$ sample with respect to the controls. Meanwhile, "Ribosome and Aminoacyl tRNA biosynthesis" and "Homologous recombination" pathways were depleted in the $T_0$ sample with respect to the controls.
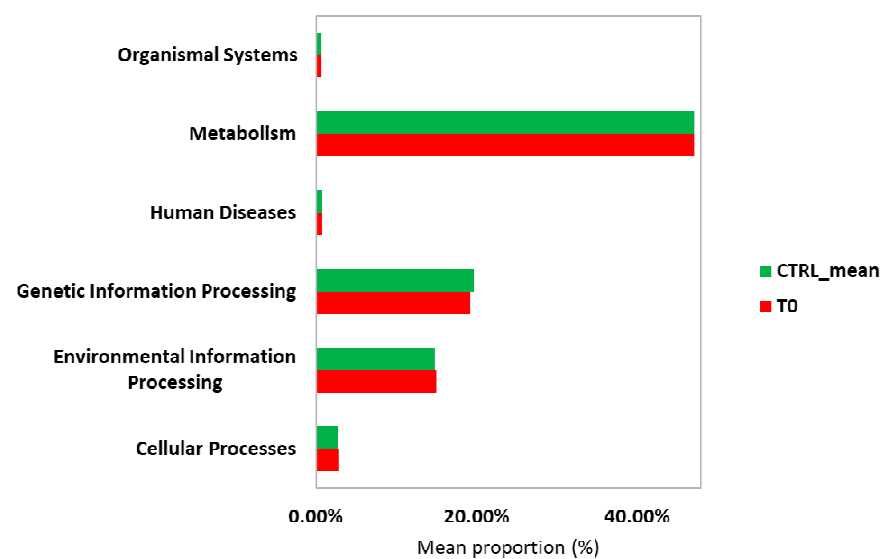


**Figure 7.** Predicted functional pathways (KEGG Level I) of the gut microbiota during infection ($T_0$) with *S. stercolaris*.
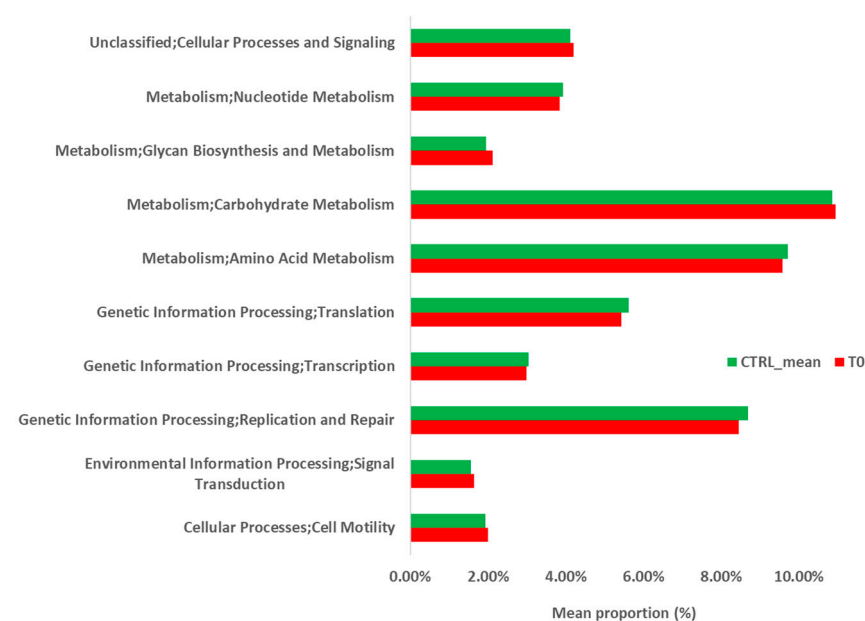


**Figure 8.** Predicted functional pathways (KEGG Level II) of the gut microbiota during infection ($T_0$) with *S. stercolaris*.

**Figure 9.** Predicted functional pathways (KEGG Level III) of the gut microbiota during infection ($T_0$) with *S. stercolaris*.

## 3. Discussion

In this report, we performed a targeted-metagenomic analysis of the gut microbiota of a seven-year-old female during and after *S. stercolaris* infection to improve our understanding of how the parasitic infection may influence the host's gut microbiota.

The patient was admitted to the Academic Department of Nephrology of the Bambino Gesù Children's Hospital for a nephrotic syndrome with several symptoms, including visual hallucinations, abdominal pain, respiratory stress, and widespread skin rash. After negative radiological exams, clinicians suspected a parasitic infection on the basis of the patient's origin and her systemic and respiratory involvements.

Several microscopic, serological, and molecular approaches were used to discern, characterize, and identify larvae in the patient's stool samples and to confirm the diagnosis. The laboratory diagnosis of strongyloidiasis was made by reporting rhabditiform larvae in the stool samples of the pediatric patient, even if in the absence of eosinophilia. However, several reports highlight that eosinophilia can be considered as a nonspecific marker for the screening of chronic strongyloidiasis, especially for individuals without severe gastrointestinal symptoms [8]. After diagnosis of strongyloidiasis, the patient received albendazole treatment for about three weeks (one day after the $T_0$ sampling point). The anti-helmintic treatment (albendazole) resulted in the resolution of the infection and in an improvement of the overall patient's health.

Regardless of the overall similarities in the composition of the patient's gut microbiota during and after parasitic infection with respect to the healthy controls at a phylum level (L2), our analysis revealed differences in the bacterial profiles of the three time-point samples ($T_0$, $T_1$, and $T_2$), thus, indicating that *S. stercoralis* infection was associated with shifts in the relative abundance of specific gut bacterial species. The alpha-diversity indices were higher in the $T_0$ and $T_1$ samples when compared to the $T_2$ sample and the average of the healthy controls. According to previous investigations, increased levels of the bacterial alpha-diversity have been reported for the gut microbiota of individuals infected by several GI helminths (i.e., *Necator americanus*, *Trichuris trichiura*, and *Ascaris* spp.) [9]. Since alpha-diversity indices are used as a proxy of the microbiota "health" (high alpha-diversity is generally associated with a stable and healthy gut bacterial environment [10]), several authors proposed that the direct or immune-mediated ability of GI helminths to promote the increase in bacterial richness and evenness may represent a therapeutic strategy in patients with chronic inflammatory disorders [11].

The differences between the patient's three time-point samples and healthy controls were displayed by dissimilarities in the relative abundance of particular bacterial taxa

in the gut microbiota profiles. As shown by the beta-diversity analysis, the $T_1$ sample is very close to the $T_0$ sample, while $T_2$ was shifted to the healthy controls. These findings suggest that anti-helminthic treatment with albendazole between $T_0$ and $T_1$ sampling points does not affect the gut microbiota composition. Accordingly, a study on Indonesian treated and untreated subjects with albendazole for helminthes infections showed that this anti-helminthic drug does not influence the composition of the gut microbiome [12].

Our results showed an enrichment of *Bifidobacterium*, *Blautia*, *Ruminococcus*, *Bacteroides*, *Corynebacterium*, *Colinsella*, *Streptococcus*, *Coprococcus*, and *Oscillospora* genera from the $T_0$ to $T_2$ time-points. Instead, *Staphylococcus*, *Lactobacillus*, and *Pediococcus* displayed a gradual depletion from the $T_0$ to $T_2$ samples.

Regarding the depletion of *Bacteroides* during *S. stercolaris* infection, one study showed that helminths infection protects mice deficient in the Crohn's disease susceptibility *Nod2* gene from intestinal abnormalities by inhibiting colonization of inflammatory *Bacteroides* species [13]. Resistance to *Bacteroides* colonization was dependent on type 2 immunity, which promoted the establishment of a protective microbiota. Bacteroidetes exhibit a crucial role in the metabolism of a wide range of carbohydrates [14]. In anaerobic environments, the products of fermentation of these substrates are short-chain fatty acids (SCFAs) that can act as a source of ATP by the host cells [15]. Additionally, SCFAs interact with the host immune system by targeting G protein coupled receptors on intestinal epithelial cells and leukocytes and modulating their development, survival, and function [16]. However, a recent study on the intestinal nematode *Trichinella spiralis* showed that *Bacteroides* genus displayed increased abundances in the *T. spiralis* positive stool samples when compared with the negative samples [17]. Therefore, these conflicting results highlight the need for further investigations in this area and that *Bacteroides* abundance during infection might depend on the parasitic species and/or on the type of host immune response.

According to our results, species belonging to the family Lactobacillaceae, which are capable of triggering host regulatory responses [18], have been widely reported to increase in abundance during helminth infection, irrespective of helminth or host species [19,20]. Moreover, several studies have demonstrated that the high abundance of *Lactobacillus* can enhance the persistence of helminth infection, providing evidence for a mutualistic relationship between helminths and *Lactobacillus* species [21,22].

We also highlighted the depletion of *Ruminococcus* genus during *S. stercoraris* infection. Accordingly, a study conducted by a shotgun metagenomics approach showed that the intestinal helminth *Trichuris suis* has an effect on the gut microbiota of pigs with a significant decrease in *Ruminococcus* [23].

Functional prediction of the bacterial metagenomic profile suggested that there was an enrichment of the "Glycan Biosynthesis" and "Carbohydrate Metabolisms" pathways during *S. stercoralis* infection ($T_0$ sample) when compared to the healthy controls. In particular, anaerobic metabolism of non-digestible carbohydrates by the gut bacteria produces short chain fatty acids (SCFAs). SCFAs, such as acetate, propionate, and butyrate, mainly in the lumen, are assumed to interact in terms of antioxidant activity, avoiding anti-inflammatory effects on the intestinal mucosa. Moreover, butyrate and propionate can regulate intestinal physiology and immune function, whereas acetate acts as a substrate for lipogenesis and gluconeogenesis [24]. Bacteroidetes and Firmicutes are the most abundant phyla in the human gut, with Bacteroidetes mainly producing acetate and propionate, while Firmicutes mostly produces butyrate [25]. Therefore, the observed enrichment of the "Carbohydrate Metabolism" pathway during parasitic infection, albeit with a low abundance of *Bacteroides*, may be explained by the high abundance of Firmicutes at the $T_0$ sampling point. Therefore, upregulation of this pathway in the gut microbiota may represent a response to oxidative stress in the host intestinal environment during *S. stercoralis* infection.

In summary, this study provides a view of changes in the gut microbiota during the course of a parasitic nematode infection. Our observational time-series experiments explored the pediatric patient's gut microbiota to elucidate the influence of parasite-related modifications and host metabolic responses to microbiota dynamics in the host intestine.

Although our findings add valuable knowledge to this emerging area of the host-parasite-microbiota interactions, agnostic multiomics-based investigations in experimental models of infection and diseases are mandatory to shed light on the contribution of the parasite-associated modifications in the gut microbiome and on the therapeutic properties of parasitic helminthes.

## 4. Case Presentation and Laboratory Diagnosis

### 4.1. Patient's Characteristics

A seven-year-old female child was admitted to the Academic Department of Nephrology of the Bambino Gesù Children's Hospital for nephrotic syndrome. The patient was born in Bolivia but adopted and transferred to Italy since May 2018. Upon admission, blood laboratory results showed haemoglobin 12.9 g/dL (11.1–14.8 g/dL), white blood cells, and full blood count within normal ranges (in particular, eosinophil count was $0.04 \times 10^3/\mu L$), while C-reactive protein was 4 mg/L (<0.50 mg/L). Her medical history included febrile episode, visual hallucinations, abdominal pain, respiratory stress, and widespread skin rash. Epidemiological and clinical data, including the systemic and respiratory involvements, suggested a parasitic infection. Hence, a collection of multiple stool samples for parasitological and gut microbiota profiling investigations was performed at three different time-points: $T_0$- during parasite infection, $T_1$- a month after parasite infection, and $T_2$- two months after parasite infection. Moreover, multiple bronchial washings and cerebrospinal fluid (CSF) samples were collected to verify the presence of parasites in other body districts.

One day after the $T_0$ sampling point, the patient received the anti-elminthic albendazole for two weeks. Therefore, at the $T_1$ point, the treatment was already ended two weeks earlier and, at $T_2$, it was ended a month and a half earlier.

This study was carried out in accordance with the recommendations of the OPBG Ethics Committee (Protocol No. 1113_OPBG_2016) and was approved on 21 April, 2016. Written informed consent was obtained from the patient and from healthy age-matched individuals, whose faecal samples were available at the BBMRI Biobank of Human Microbiome of the Bambino Gesù Children's Hospital.

### 4.2. Laboratory Diagnosis of Strongyloidiasis

#### 4.2.1. Optical Microscopy

The laboratory diagnosis of strongyloidiasis was made by optical microscopy characterization of larvae in a fecal specimen. With this purpose, fecal samples were concentrated by an ethyl acetate-based technique and examined under light microscopy at 20× and 40× magnification. The assessment of the morphological characteristics of the larvae was made on a smear of feces stained by Lugol independently by two parasitologists.

#### 4.2.2. Stool Agar Culture

Stool samples were also tested for direct parasite searching through the culture onto *S. stercoralis* Agar (Biolife Italiana s.r.l., Milano). The agar plate culture was performed using approximately 3–5 g of feces and the plates were sealed with adhesive tape to prevent larvae from crawling out of the plate and were incubated at 30 °C for at least 7 days [26].

#### 4.2.3. Immunological Methods

Qualitative detection of IgG to *S. stercoralis* was performed using an enzyme-linked immunosorbent assay based on micro-wells coated with *Strongyloides* antigen (ELISA, S. ratti Bordier Products, Effegiemme).

#### 4.2.4. DNA Extraction and PCR Amplification for *S. stercoralis* Detection

Genomic DNA was extracted from stool by using a QIAamp Fast DNA Stool Mini Kit (Qiagen, Germany) with a slight method modification based on the addition of 1 mL of Inhibit EX buffer (Qiagen, Germany) to the sample heated at 70 °C for 5 min in order to increase the quality of extracted DNA. The DNA was finally eluted with 200 μL ATE buffer.

The PCR reactions were performed using the following reaction mixture: 22 μL master mix, (Faststart HIFI PCR SYST.DNTP 500U SIGMA-ALDRICH S.r.L.) 1 μL of each primer (forward: 5′ ATC GTG TCG GTG GAT CAT TC 3′, reverse: 5′ CTA TTA GCG CCA TTT GCA TTC 3′), 3 μL of DNA template, and ultra-pure bi-distilled $H_2O$ up to a final volume of 30 μL under the following conditions: 1 cycle at 95 °C for 5 min (time-delay), 30 cycle at 94 °C for 30s (denaturation), 58 °C for 45 s (annealing), and 72 °C for 45 s (extension), which is followed by a final extension for 5 min [27]. DNA extracted from stool samples of pediatric patients infected with filariform larvae was used as positive controls, while DNA extracted from microscopically negative samples and ultra-pure bi-distilled $H_2O$ was used as a negative control of the PCR reaction.

### 4.3. Gut Microbiota Profiling by 16S rRNA Targeted-Metagenomics Sequencing

### 4.3.1. Bacterial DNA Extraction from Stool Samples

Stool samples were pre-treated by a bead-beating process using 0.1-mm glass beads. This step is crucial because it enables the mechanical disruption of bacteria otherwise difficult to lyse using chemical/enzymatic buffers.

Subsequently, DNA from stool samples was extracted using QIAmp Fast DNA Stool mini kit (Qiagen, Hilden, Germany), according to the manufacturer's instructions. Sixteen stool samples from healthy, age-matched individuals were used as a gut microbiota reference for comparisons. We checked the purity of extracted DNA by Nanodrop measurements (Thermo Fisher Scientific, Waltham, MA, USA). Samples that failed quality control (DNA yield and purity not adequate for libraries preparation) were re-extracted. Amplification of the variable V3–V4 regions from the 16S rRNA bacterial gene (∼460 bp) was carried out using the primer pairs 16S_F 5′-(TCG TCG GCA GCG TCA GAT GTG TAT AAG AGA CAG CCT ACG GGN GGC WGC AG)-3′ and 16S_R 5′-(GTC TCG TGG GCT CGG AGA TGT GTA TAA GAG ACA GGA CTA CHV GGG TAT CTA ATC C)-3′ as described in the MiSeq rRNA Amplicon Sequencing protocol (Illumina, San Diego, CA, USA). The polymerase chain reaction (PCR) was set up by using the 2× KAPA Hifi HotStart ready Mix kit (KAPA Biosystems Inc., Wilmington, MA, USA). DNA amplicons were cleaned-up by the CleanNGS kit beads (CleanNA, Coenecoop 75, 2741 PH, Waddinxveen, The Netherlands). A second amplification step was performed to obtain a unique combination of dual Illumina Nextera XT indices and adaptor primers. The final library was cleaned-up using CleanNGS kit beads, quantified using Quant-iT PicoGreen dsDNA Assay Kit (Thermo Fisher Scientific, Waltham, MA, USA), normalized and diluted to equimolar concentrations (4 nmol/L). The size of the libraries (600–630 bp) was checked using 2100 Bioanalyzer Desktop System (Agilent Technologies Inc., Santa Clara, CA, USA). Pooled and denatured libraries were sequenced by a MiSeq Reagent Kit v2 (300 cycles) (Illumina Inc., San Diego, CA, USA) on the MiSeqDX Instrument (Illumina Inc., San Diego, CA, USA).

### 4.3.2. Bioinformatics Analysis

The Illumina sequence raw data were processed using QIIME version 1.9.1 [28]. The workflow started with joined paired-end reads, quality filtering, and library splitting, followed by the detection of the chimeric sequences with the UCHIME algorithm, included in the free version of USEARCH61, and the subsequent removal prior to further analysis.

Cleaned reads were clustered and assigned to operational taxonomic units (OTUs) against the Greengenes 13.8 database [29] with a 97% identity threshold using an open-reference OTU-picking protocol with "usearch". OTUs were then further normalized using metagenome Seq's CSS (cumulative sum scaling) transformation and, finally, taxa below a minimum fractional count of 0.01% were filtered from the OTU table.

To highlight differences between the patient's three time-points' samples and the controls in term of bacteria abundances, we performed several heatmaps with hierarchical clustering (clustering metric: "correlation" and method: "complete") in R v.4.0.2 environment using Pheatmap package (https://cran.r-project.org/web/packages/pheatmap/pheatmap.pdf (accessed on 20 February 2021)).

Alpha-diversity was estimated by calculating the Shannon and Observed species indices. Beta-diversity was assessed by calculating the Bray-Curtis dissimilarity index. Differences in community composition were visualized by performing principle coordinate analysis (PCoAs). The molecular functions of the bacterial communities were predicted using the Phylogenetic Investigation of Communities by Reconstruction of Unobserved States (PICRUSt) [30] based on 16S rRNA metadata with the Kyoto encyclopedia of genes and genomes (KEGG) database and Greengenes 13.8 reference taxonomy [31].

**Author Contributions:** Conception and design: S.P., A.S., A.I., and L.P. Analysis and validation: A.S. and A.I. Clinical evaluation of the patient: S.P. and L.R. Manuscript writing: S.P., A.I., and L.P. All authors have read and agreed to the published version of the manuscript.

**Institutional Review Board Statement:** The study was conducted according to the guidelines of the Declaration of Helsinki and all methods were performed in accordance with the relevant guidelines and regulations. This study was carried out in accordance with the recommendations of the OPBG Ethics Committee (Protocol No. 1113_OPBG_2016) and was approved on 21 April 2016.

**Informed Consent Statement:** Written informed consent was obtained from the patient and from healthy age-matched individuals, whose faecal samples were available at the BBMRI Biobank of Human Microbiome of the Bambino Gesù Children's Hospital.

**Data Availability Statement:** The data that support the findings of this study are available on request from the corresponding author.

**Conflicts of Interest:** The authors declare no conflict of interest.

# References

1. Bisoffi, Z.; Buonfrate, D.; Montresor, A.; Requena-Mendez, A.; Munoz, J.; Krolewiecki, A.J.; Gotuzzo, E.; Mena, M.A.; Chiodini, P.L.; Anselmi, M.; et al. Strongyloides stercoralis: A plea for action. *PLoS Neglect. Trop. D* **2013**, *7*, e2214. [CrossRef]
2. Nutman, T.B. Human infection with Strongyloides stercoralis and other related Strongyloides species. *Parasitology* **2017**, *144*, 263–273. [CrossRef] [PubMed]
3. Buonfrate, D.; Baldissera, M.; Abrescia, F.; Bassetti, M.; Caramaschi, G.; Giobbia, M.; Mascarello, M.; Rodari, P.; Scattolo, N.; Napoletano, G.; et al. Epidemiology of Strongyloides stercoralis in northern Italy: Results of a multicentre case-control study, February 2013 to July 2014. *Eurosurveillance* **2016**, *21*, 30310. [CrossRef] [PubMed]
4. Albarqi, M.M.Y.; Stoltzfus, J.D.; Pilgrim, A.A.; Nolan, T.J.; Wang, Z.; Kliewer, S.A.; Mangelsdorf, D.J.; Lok, J.B. Regulation of Life Cycle Checkpoints and Developmental Activation of Infective Larvae in Strongyloides stercoralis by Dafachronic Acid. *PLoS Pathog* **2016**, *12*, e1005358. [CrossRef]
5. Csermely, L.; Jaafar, H.; Kristensen, J.; Castella, A.; Gorka, W.; Chebli, A.A.; Trab, F.; Alizadeh, H.; Hunyady, B. Strongyloides hyper-infection causing life-threatening gastrointestinal bleeding. *World J. Gastroenterol.* **2006**, *12*, 6401–6404. [CrossRef] [PubMed]
6. Kuo, C.-E.; Chuah, S.-K.; Tai, W.-C.; Lee, C.-H. Upper gastrointestinal bleeding caused by Strongyloides stercoralis: Highlighting a neglected parasitic infection. *Kaohsiung J. Med. Sci.* **2017**, *33*, 269–270. [CrossRef] [PubMed]
7. Marcos, L.A.; Terashima, A.; Dupont, H.L.; Gotuzzo, E. Strongyloides hyperinfection syndrome: An emerging global infectious disease. *Trans. R. Soc. Trop Med. Hyg.* **2008**, *102*, 314–318. [CrossRef] [PubMed]
8. Teixeira, M.C.A.; Pacheco, F.T.F.; Souza, J.N.; Silva, M.L.S.; Ines, E.J.; Soares, N.M. Strongyloides stercoralis Infection in Alcoholic Patients. *Biomed. Res. Int.* **2016**, *2016*, 4872473. [CrossRef]
9. Jenkins, T.P.; Formenti, F.; Castro, C.; Piubelli, C.; Perandin, F.; Buonfrate, D.; Otranto, D.; Griffin, J.L.; Krause, L.; Bisoffi, Z.; et al. A comprehensive analysis of the faecal microbiome and metabolome of Strongyloides stercoralis infected volunteers from a non-endemic area. *Sci. Rep.-UK* **2018**, *8*, 15651. [CrossRef] [PubMed]
10. Menni, C.; Jackson, M.A.; Pallister, T.; Steves, C.J.; Spector, T.D.; Valdes, A.M. Gut microbiome diversity and high-fibre intake are related to lower long-term weight gain. *Int. J. Obes.* **2017**, *41*, 1099–1105. [CrossRef]
11. Zaiss, M.M.; Rapin, A.; Lebon, L.; Dubey, L.K.; Mosconi, I.; Sarter, K.; Piersigilli, A.; Menin, L.; Walker, A.W.; Rougemont, J.; et al. The Intestinal Microbiota Contributes to the Ability of Helminths to Modulate Allergic Inflammation. *Immunity* **2015**, *43*, 998–1010. [CrossRef] [PubMed]

12. Martin, I.; Djuardi, Y.; Sartono, E.; Rosa, B.A.; Supali, T.; Mitreva, M.; Houwing-Duistermaat, J.J.; Yazdanbakhsh, M. Dynamic changes in human-gut microbiome in relation to a placebo-controlled anthelminthic trial in Indonesia. *PLoS Neglect. Trop. D* **2018**, *12*, e0006620. [CrossRef]

13. Ramanan, D.; Bowcutt, R.; Lee, S.C.; Tang, M.S.; Kurtz, Z.D.; Ding, Y.; Honda, K.; Gause, W.C.; Blaser, M.J.; Bonneau, R.A.; et al. Helminth infection promotes colonization resistance via type 2 immunity. *Science* **2016**, *352*, 608–612. [CrossRef] [PubMed]

14. Thomas, F.; Hehemann, J.-H.; Rebuffet, E.; Czjzek, M.; Michel, G. Environmental and gut bacteroidetes: The food connection. *Front. Microbiol.* **2011**, *2*, 93. [CrossRef]

15. den Besten, G.; van Eunen, K.; Groen, A.K.; Venema, K.; Reijngoud, D.-J.; Bakker, B.M. The role of short-chain fatty acids in the interplay between diet, gut microbiota, and host energy metabolism. *J. Lipid Res.* **2013**, *54*, 2325–2340. [CrossRef]

16. Correa-Oliveira, R.; Fachi, J.L.; Vieira, A.; Sato, F.T.; Vinolo, M.A.R. Regulation of immune cell function by short-chain fatty acids. *Clin. Transl. Immunology* **2016**, *5*, e73. [CrossRef]

17. Liu, S.; Pan, J.; Meng, X.; Zhu, J.; Zhou, J.; Zhu, X. Trichinella spiralis infection decreases the diversity of the intestinal flora in the infected mouse. *J. Microbiol. Immunol. Infect.* **2019**. [CrossRef] [PubMed]

18. Brosschot, T.P.; Reynolds, L.A. The impact of a helminth-modified microbiome on host immunity. *Mucosal. Immunol.* **2018**, *11*, 1039–1046. [CrossRef] [PubMed]

19. Holm, J.B.; Sorobetea, D.; Kiilerich, P.; Ramayo-Caldas, Y.; Estelle, J.; Ma, T.; Madsen, L.; Kristiansen, K.; Svensson-Frej, M. Chronic Trichuris muris Infection Decreases Diversity of the Intestinal Microbiota and Concomitantly Increases the Abundance of Lactobacilli. *PLoS ONE* **2015**, *10*, e0125495. [CrossRef]

20. Kreisinger, J.; Bastien, G.; Hauffe, H.C.; Marchesi, J.; Perkins, S.E. Interactions between multiple helminths and the gut microbiota in wild rodents. *Philos Trans. R. Soc. Lond. B Biol. Sci.* **2015**, *370*, 20140295. [CrossRef]

21. Reynolds, L.A.; Smith, K.A.; Filbey, K.J.; Harcus, Y.; Hewitson, J.P.; Redpath, S.A.; Valdez, Y.; Yebra, M.J.; Finlay, B.B.; Maizels, R.M. Commensal-pathogen interactions in the intestinal tract: Lactobacilli promote infection with, and are promoted by, helminth parasites. *Gut. Microbes* **2014**, *5*, 522–532. [CrossRef]

22. Walk, S.T.; Blum, A.M.; Ewing, S.A.-S.; Weinstock, J.V.; Young, V.B. Alteration of the murine gut microbiota during infection with the parasitic helminth Heligmosomoides polygyrus. *Inflamm. Bowel. Dis.* **2010**, *16*, 1841–1849. [CrossRef]

23. Lee, S.C.; Tang, M.S.; Lim, Y.A.L.; Choy, S.H.; Kurtz, Z.D.; Cox, L.M.; Gundra, U.M.; Cho, I.; Bonneau, R.; Blaser, M.J.; et al. Helminth colonization is associated with increased diversity of the gut microbiota. *PLoS Neglect. Trop. D* **2014**, *8*, e2880. [CrossRef] [PubMed]

24. Vernocchi, P.; Del Chierico, F.; Putignani, L. Gut Microbiota Metabolism and Interaction with Food Components. *Int. J. Mol. Sci.* **2020**, *21*, 3688. [CrossRef] [PubMed]

25. Parada Venegas, D.; De la Fuente, M.K.; Landskron, G.; Gonzalez, M.J.; Quera, R.; Dijkstra, G.; Harmsen, H.J.M.; Faber, K.N.; Hermoso, M.A. Short Chain Fatty Acids (SCFAs)-Mediated Gut Epithelial and Immune Regulation and Its Relevance for Inflammatory Bowel Diseases. *Front. Immunol.* **2019**, *10*, 277. [CrossRef]

26. Koga, K.; Kasuya, S.; Ohtomo, H. How effective is the agar plate method for Strongyloides stercoralis? *J. Parasitol.* **1992**, *78*, 155–156. [CrossRef] [PubMed]

27. Moghaddassani, H.; Mirhendi, H.; Hosseini, M.; Rokni, M.; Mowlavi, G.; Kia, E. Molecular Diagnosis of Strongyloides stercoralis Infection by PCR Detection of Specific DNA in Human Stool Samples. *Iran. J. Parasitol.* **2011**, *6*, 23–30.

28. Caporaso, J.G.; Kuczynski, J.; Stombaugh, J.; Bittinger, K.; Bushman, F.D.; Costello, E.K.; Fierer, N.; Pena, A.G.; Goodrich, J.K.; Gordon, J.I.; et al. QIIME allows analysis of high-throughput community sequencing data. *Nat. Methods* **2010**, *7*, 335–336. [CrossRef]

29. Yokono, M.; Satoh, S.; Tanaka, A. Comparative analyses of whole-genome protein sequences from multiple organisms. *Sci. Rep.-UK* **2018**, *8*, 6800. [CrossRef] [PubMed]

30. Langille, M.G.I.; Zaneveld, J.; Caporaso, J.G.; McDonald, D.; Knights, D.; Reyes, J.A.; Clemente, J.C.; Burkepile, D.E.; Vega Thurber, R.L.; Knight, R.; et al. Predictive functional profiling of microbial communities using 16S rRNA marker gene sequences. *Nat. Biotechnol.* **2013**, *31*, 814–821. [CrossRef]

31. DeSantis, T.Z.; Hugenholtz, P.; Larsen, N.; Rojas, M.; Brodie, E.L.; Keller, K.; Huber, T.; Dalevi, D.; Hu, P.; Andersen, G.L. Greengenes, a chimera-checked 16S rRNA gene database and workbench compatible with ARB. *Appl. Environ. Microbiol.* **2006**, *72*, 5069–5072. [CrossRef] [PubMed]